



1 **Investigation of spatial and temporal variability in lower tropospheric ozone**
2 **from RAL Space UV-Vis satellite products**

3 Richard J. Pope^{1,2}, Brian J. Kerridge^{3,4}, Richard Siddans^{3,4}, Barry G. Latter^{3,4}, Martyn P. Chipperfield^{1,2}, Wuhu
4 Feng^{1,5}, Matilda A. Pimlott¹, Sandip S. Dhomse^{1,2}, Christian Retscher⁶ and Richard Rigby^{1,7}

5 *1: School of Earth and Environment, University of Leeds, Leeds, United Kingdom*

6 *2: National Centre for Earth Observation, University of Leeds, Leeds, United Kingdom*

7 *3: Remote Sensing Group, STFC Rutherford Appleton Laboratory, Chilton, United Kingdom*

8 *4: National Centre for Earth Observation, STFC Rutherford Appleton Laboratory, Chilton, United Kingdom*

9 *5: National Centre for Atmospheric Science, University of Leeds, Leeds, United Kingdom*

10 *6: European Space Agency, ESRI, Frascati, Italy*

11 *7: Centre for Environmental Modelling and Computation, University of Leeds, Leeds, United Kingdom*

12

13 *Correspondence to: Richard J. Pope (r.j.pope@leeds.ac.uk)*

14 **Key Points**

- 15 • The RAL Space profile retrieval algorithm for ultraviolet-visible nadir sounders has good vertical
16 sensitivity to retrieve lower tropospheric column ozone (LTCO₃).
- 17 • OMI, SCIAMACHY and GOME-1 have suitably stable LTCO₃ records in comparison to ozonesondes
18 and are merged to form the first long-term satellite LTCO₃ record (1996-2017).
- 19 • Comparison of 5-year averages for 1996-2000 and 2013-2017 suggests a significant LTCO₃ increase
20 (3.0 to 5.0 DU) in the tropics/sub-tropics over the satellite-era.
21

22 **Abstract:**

23 Ozone is a potent air pollutant in the lower troposphere and an important short-lived climate forcer (SLCF) in
24 the upper troposphere. Studies using satellite data to investigate spatiotemporal variability of troposphere
25 ozone (TO₃) have predominantly focussed on the tropospheric column metric. This is the first study to
26 investigate long-term spatiotemporal variability in lower tropospheric column ozone (LTCO₃, surface-450 hPa
27 sub-column) by merging multiple European Space Agency – Climate Change Initiative (ESA-CCI) products
28 produced by the Rutherford Appleton Laboratory (RAL) Space. We find that in the LTCO₃, the degrees of
29 freedom of signal (DOFS) from these products varies with latitude range and season and is up to 0.65,
30 indicating that the retrievals contain useful information on lower TO₃. The spatial and seasonal variation of
31 the RAL Space products are in good agreement with each other but there are systematic offsets of up to 3.0-
32 5.0 DU between them. Comparison with ozonesondes shows that the Global Ozone Monitoring Experiment
33 (GOME-1, 1996-2003), the SCanning Imaging Absorption spectroMeter for Atmospheric
34 CartographY (SCIAMACHY, 2003-2010) and the Ozone Monitoring Instrument (OMI, 2005-2017) have stable
35 LTCO₃ records over their respective periods, which can be merged together. While GOME-2 (2008-2018)
36 shows substantial drift in its bias with respect to ozonesondes. We have therefore constructed a robust
37 merged dataset of LTCO₃ from GOME-1, SCIAMACHY and OMI between 1996 and 2017. Comparing the
38 LTCO₃ differences between the 1996-2000 and 2013-2017 5-year averages, we find significant positive
39 increases (3.0-5.0 DU) in the tropics/sub-tropics, while in the northern mid-latitudes, we find small scale



40 differences in LTCO₃. Therefore, we conclude that there has been a substantial increase in tropical/sub-
41 tropical LTCO₃ during the satellite-era.

42 1. Introduction

43 Tropospheric ozone (TO₃) is a short-lived climate forcer (SLCF) and, is the third most important greenhouse
44 gas (GHG; e. g. Myhre et al., 2013). TO₃ is also a hazardous air pollutant with adverse impacts on human
45 health (WHO, 2018) and the biosphere (e.g. agricultural and natural vegetation; Sitch et al., 2007). Since the
46 pre-industrial (PI) period, anthropogenic activities have increased the atmospheric loading of ozone (O₃)
47 precursor gases, most notably nitrogen oxides (NO_x) and methane (CH₄), resulting in a substantial increase in
48 TO₃ of 25-50% since 1900 (Gauss et al., 2006; Lamarque et al., 2010; Young et al., 2013). The PI to present
49 day (PD) radiative forcing (RF) from TO₃ is estimated by the Intergovernmental Panel on Climate Change
50 (IPCC) to be 0.4 Wm⁻² (Myhre et al., 2013; Stevenson et al., 2013) with an uncertainty range of 0.2-0.6 Wm⁻².

51 During the satellite-era, with a number of missions since 2000, extensive records of TO₃ have been
52 produced, e.g. by the European Space Agency Climate Change Initiative (ESA-CCI; ESA, 2019). However, the
53 large overburden of stratospheric O₃, coupled with the different vertical sensitivities and sources of error
54 associated with observations in different wavelength regions (e.g. Eskes and Boersma 2003; Ziemke et al.,
55 2011; Miles et al., 2015) contributes to large-scale spatiotemporal inconsistencies between the records
56 (Gaudel et al., 2018). So, various studies (e.g. Heue et al. 2016; Pope et al., 2018; Ziemke et al. 2019)
57 analysing TO₃ trends usually focussed one or two instruments. The work by Gaudel et al. (2018) was part of
58 the Tropospheric Ozone Assessment Report (TOAR), which represented a large global effort to understand
59 spatiotemporal patterns and variability in TO₃. Gaudel et al., 2018 analysed ozonesondes and multiple polar
60 orbiting-nadir viewing satellite products and reported that there is large-scale discrepancies in the spatial
61 distribution, magnitude, direction and significance of the TCO₃ trends. While the satellite records did cover
62 slightly different time periods, they were unable to provide any definitive reasons for these discrepancies
63 beyond briefly suggesting that differences in measurement techniques and retrieval methods were likely to
64 be causing the observed spatial inconsistencies.

65 The vertical sensitivity of each product (function of measurement technique and retrieval methodology)
66 used by Gaudel et al. (2018) has a substantial impact on which part of the troposphere (and stratosphere)
67 the O₃ signal is weighted towards. The vertical sensitivity/weighting function can be referred to as the
68 “averaging kernel” (AK), which provides the relationship between perturbations at different levels in the
69 retrieved and true profiles (Rodgers, 2000; Eskes and Boersma, 2003). As the instruments’ vertical
70 sensitivities differ so might the processes controlling variability in retrieved TO₃ and so trends may also differ
71 between products.

72 In this study, we explore the spatiotemporal variability of lower tropospheric column ozone (LTCO₃, surface
73 to 450 hPa) from several ultraviolet-visible (UV-Vis) sounders produced by Rutherford Appleton Laboratory
74 (RAL) Space. While Gaudel et al., (2018) used a range of UV-Vis and infrared (IR) TCO₃ products, including the
75 RAL Space Ozone Monitoring Instrument (OMI) product, we focus here on several RAL Space UV-Vis
76 products. Here, we aim to explore the consistencies between them, their vertical sensitivities, LTCO₃ stability
77 against ozonesonde records and suitability for long-term trend analysis. In our manuscript, section 2
78 discusses the satellite/ozonesonde datasets, section 3 presents are results and our conclusions/discussion
79 are summarised in section 4.

80

81



82 **2. Methodology and Datasets**

83 **2.1. Datasets**

84 The four RAL Space UV-Vis satellite products investigated here are from OMI, the Global Ozone Monitoring
85 Experiment – 1 (GOME-1), GOME-2 and the Scanning Imaging Absorption spectroMeter for Atmospheric
86 Cartography (SCIAMACHY), all of which were developed as part of the ESA-CCI project (**Table 1**). GOME-1,
87 GOME-2, SCIAMACHY and OMI flew on ESA's ERS-2, MetOp-A, ENVISAT and NASA's Aura satellites in sun-
88 synchronous low Earth polar orbits with local overpass times of 10.30, 9.30, 10.00 and 13.30, respectively.
89 They are all nadir viewing with spectral ranges which include the 270-350 nm range used for ozone profile
90 retrieval. The spatial footprints of the respective instruments at nadir are 320 km × 40 km, 80 km × 40 km,
91 240 km × 30 km and 24 km × 13 km (Boersma et al., 2011; Miles et al., 2015; Shah et al., 2018). The scheme
92 established by RAL Space to retrieve ozone height-resolved O₃ profiles with tropospheric sensitivity (Miles et
93 al., 2015) was applied to all of these satellite instruments¹. The scheme is based on the optimal estimation
94 (OE) approach of Rogers et al., (2000) and provides state-of-the-art retrieval sensitivity to lower TO₃, which is
95 described in detail by Miles et al., (2015) and by Keppens et al., (2018). For this work, the data were filtered
96 for good quality retrievals whereby the geometric cloud fraction was <0.2, the lowest sub-column O₃ value
97 was > 0.0, the solar zenith angle < 80.0°, the convergence flag = 1.0 and the normalised cost function was <
98 2.0. The OMI, GOME-1, GOME-2 and SCIAMACHY level 2 data were aggregated on a 1.0°×1.0° spatial grid
99 using the gridding approach of Pope et al., (2018).

100 **2.2. Ozonesondes and Application of Satellite Averaging Kernels**

101 To help understand the impact of the satellite AKs on retrieved LTCO₃ and stability of the satellite
102 instruments listed in **Table 1** over time, we use ozonesonde data between 1995 and 2019 from the World
103 Ozone and Ultraviolet Radiation Data Centre (WOUDC), the Southern Hemisphere ADditional Ozonesondes
104 (SHADOZ) project and from the National Oceanic and Atmospheric Administration (NOAA). Keppens et al.,
105 (2018) undertook a detailed assessment of the ESA-CCI TO₃ data sets, including the RAL UV-Vis profile data
106 sets used in this study (mostly older versions though) using ozonesondes. They found that the RAL LTCO₃
107 products typically had a positive bias of about 40%, apart from OMI which was closer to 10%. On the global
108 scale, tropospheric drift in GOME-1 and OMI over time was approximately -5% and 10% per decade,
109 respectively. However, GOME-2 and SCIAMACHY had significant tropospheric drift trends of approximately
110 40% per decade. The recent Copernicus *Product Quality Assessment Report (PQAR) Ozone Products Version*
111 *2.0b* (Copernicus, 2021) undertook a more recent assessment of nadir ozone profiles using the level 3
112 products of the RAL and IASI-FORLI product listed in **Table 1**. They found that in the troposphere,
113 OMI/GOME-1 and SCIAMACHY/GOME-2 had biases of -20% and 10%. GOME-1 tropospheric drift was deemed
114 to be insignificant (-10% to 5% per decade), while GOME-2 and SCIAMACHY had a significant drift of 30% and
115 20% per decade, respectively. OMI also had an insignificant tropospheric drift of 10% per decade.

116 In this study, for comparisons between ozonesonde profiles and satellite retrievals, each ozonesonde profile
117 was spatiotemporally co-located within 500 km and 6-hours to allow for robust comparisons and reduce
118 representation errors. Here, ozonesonde O₃ measurements were rejected if the O₃ or pressure values were
119 unphysical (i.e. < 0.0), if the O₃ partial pressure > 2000.0 mPa or the O₃ value was set to 99.9, and whole
120 ozonesonde profiles were rejected if at least 50% of the measurements did not meet these criteria. These
121 criteria are similar to those applied by Keppens et al., (2018) and Hubert et al., (2016). To allow for direct
122 like-for-like comparisons between the two quantities, accounting for the vertical sensitivity of the satellite,

¹ The version applied in producing this version of OMI data differed in several respects from that applied to the other three sensors, which might perhaps contribute to inter-instrument bias.



123 the instrument AKs were applied the ozonesonde profiles. Here, each co-located ozonesonde profile (in
124 volume mixing ratio) was used to derive ozone sub-columns (in number density) on the satellite pressure
125 grid. The application of the AKs for the UV-Vis instruments was done using **Equation 1**:

$$126 \quad \text{sonde}_{AK} = AK \cdot (\text{sonde}_{int} - apr) + apr \quad (1)$$

127 where sonde_{AK} is the modified ozonesonde sub-column profile (Dobson units, DU), AK is the averaging kernel
128 matrix, sonde_{int} is the sonde sub-column profile (DU) on the satellite pressure grid and apr is the a priori sub-
129 column amount (DU).

130 3. Results

131 3.1. Satellite Vertical Sensitivity

132 **Figure 1** represents average AKs for all the instruments listed in **Table 1** for 2008 (1998 for GOME-1) in the
133 northern (NH) and southern (SH) hemispheres. Of the four RAL Space products, OMI O₃ profiles appear to
134 contain most information with degrees of freedom of signal (DOFS) of 5.0 or above for the full atmosphere
135 (DOFS also presented in **Table 2**). SCIAMACHY has the lowest sensitivity with average DOFS ranging between
136 4.13 and 4.65. The DOFS tend to be larger in NH for all the products, though there is no clear pattern in the
137 seasonality (i.e. January vs. July). In terms of LTCO₃, OMI again has greater sensitivity than the others with
138 average hemispheric and seasonal DOFS ranging between 0.53 and 0.65. For GOME-1 (GOME-2), the LTCO₃
139 DOFS range between 0.38 and 0.50 (0.24 and 0.45). SCIAMACHY LTCO₃ DOFS range between 0.44 and 0.51.
140 Therefore, while SCIAMACHY has the lowest overall sensitivity to full atmosphere ozone, it has reasonably
141 good information in the LTCO₃. GOME-2 has the least vertical sensitivity to LTCO₃, especially in SH summer at
142 0.24. As a result, GOME-2 LTCO₃ is more influenced by the a priori, especially in SH summer, as illustrated in
143 **Figure 1**.

144 This is investigated further by co-locating the products with the merged ozonesonde data set, over their
145 respective mission periods, globally and in the NH and SH (**Figure 2**). For all the instruments, there are
146 suitable samples sizes (N > 1000 in all cases) of co-located retrievals and derived ozonesonde LTCO₃. In the
147 case of GOME-1, the global distribution has a 25th-75th percentile (25_75%) range of approximately 8.0 to
148 20.0 DU and a median of 14.0 DU. The a priori 25_75% range and median values are 16.0 to 22.0 and 19.0
149 DU. These substantial differences between retrieved and a priori values confirm there is sensitivity in the
150 GOME-1 retrieval to lower tropospheric ozone. It can be seen from **Equation 1** that if a satellite instrument
151 had perfect sensitivity at all levels (i.e. AK=1), there would be no change in co-located ozonesonde LTCO₃
152 distribution when the AKs are applied. However, given AK values are less than 1.0 in **Figure 1**, leading to the
153 DOFS of approximately 0.5, there is a shift in the median value towards the a priori from approximately 21.0
154 to 19.0 DU. The corresponding ozonesonde 10th-90th percentile (10_90%) range 13.0 to 26.0 DU expanded to
155 12.0 to 27.0 DU. Therefore, the application of the AKs to the ozonesondes actually increases the range of
156 observed values. In the NH, the GOME-1 median (25_75% range) is 14.0 (4.0-24) DU while the a priori median
157 (25_75% range) is 21.0 (18.0-23.0) DU. The ozonesonde median (25_75% range) is 22.0 (19.0-25.0) DU while
158 application of the AKs yields values of 19.0 (16.0-24.0) DU. In the SH, the GOME-1 median (25_75% range) is
159 12.0 (8.0-17.0) DU while the a priori median (25_75% range) is 14.0 (12.0-16.0) DU. The ozonesonde median
160 (25_75% range) is 12.0 (11.0-17.0) DU while application of the AKs yields values of 12.0 (6.0->40.0) DU. In
161 comparison, GOME-2 shows a similar response though the shift in LTCO₃ value between the a priori and
162 satellite is smaller. This makes sense given the lower LTCO₃ DOFS for GOME-2. In the SH, the application of
163 the AKs to the ozonesondes yields a very large range in the percentiles. It is likely that the South Atlantic
164 Anomaly (SAA – i.e. where charged particles directly impact UV detectors increasing dark-current noise,
165 which in turn reduces the number of retrievals from all UV sensors, notably both GOME-1 and GOME-2;



166 Keppens et al., 2018), given the typically larger values and signal corruption, is driving the large response in
167 the ozonesonde+AKs range.

168 For OMI, the global distribution has a median (25_75% range) of 17.0 (13.0-25.0) DU yielding a substantial
169 shift from the apriori median (25_75% range) of 18.0 (16.0-22.0) DU. In the NH, the satellite median (25_75%
170 range) is 18.0 (13.0-25.0) DU and the apriori median (25_75% range) value is 20.0 (17.0-23.0) DU. In the SH,
171 the satellite median (25_75% range) is 14.0 (10.0-22.0) DU and the apriori median (25_75% range) value of
172 15.0 (13.0-19.0) DU. When the AKs are applied to the ozonesondes there is typically an increase in the
173 median L_{TCO₃} and range by approximately 3.0-4.0 DU. For SCIAMACHY, a similar relationship occurs with a
174 shift of the satellite L_{TCO₃} median away from the apriori by 1.0-3.0 DU and an increase in the 25_75% range
175 by 10.0-15.0 DU. Apart from the SH, the application of the AKs to the ozonesondes shifts the L_{TCO₃} median
176 by 2.0-3.0 DU but the 25_75% range remains similar. Overall, there is a shift in the satellite L_{TCO₃} median
177 value away from the apriori with an increase in the 25_75% and 10_90% ranges. A similar pattern occurs in
178 multiple cases between the ozonesondes and the ozonesondes+AKs. Therefore, all the instruments have
179 reasonable vertical sensitivity in L_{TCO₃} with substantial perturbations from the apriori and to the satellite
180 L_{TCO₃} distribution.

181 3.2. Lower Tropospheric Column Ozone Seasonality

182 Multiple studies have investigated the seasonality of TO₃ from space observing large biomass burning and
183 lightning induced O₃ in the South Atlantic (Ziemke et al., 2006; Ziemke et al., 2011; Pope et al., 2020),
184 enhanced summertime TO₃ over the Mediterranean (Richards et al., 2013), TO₃ over large precursor regions
185 such as China and India (Verstraeten et al., 2015) and the enriched northern hemispheric background O₃
186 during springtime (Ziemke et al., 2006). Here, we compare the long-term seasonal (December-January-
187 February, DJF, and June-July-August, JJA) spatial distributions of RAL Space L_{TCO₃} products (**Figure 3**).

188 OMI and GOME-2 L_{TCO₃} have regions of consistency (e.g. JJA NH enhanced background TO₃, between 20.0
189 DU and 30.0 DU, and the Mediterranean TO₃ peak, >25.0 DU), but the SAA interferes with the signal of the
190 biomass burning induced secondary O₃ formation from Africa and South America. However, for OMI, this
191 ozone plume ranges between 23.0 and 27.0 DU (18.0 and 20.0 DU) in DJF (JJA). There are also clear L_{TCO₃}
192 hotspots over anthropogenic regions (e.g. eastern China and northern India) peaking at over 25.0 DU in JJA.
193 The GOME-1 L_{TCO₃} spatial patterns are consistent with that of OMI and GOME-2, but there is a systematic
194 low bias relative to OMI and GOME-2 in the absolute L_{TCO₃} of 3.0 DU to 7.0 DU, depending on geographical
195 location (e.g. 20.0-22.0 DU over northern India for GOME-2 and OMI, while 16-18 DU for GOME-1). The
196 SCIAMACHY spatial pattern and absolute L_{TCO₃} values are more consistent with OMI and GOME-2.
197 Moreover, SCIAMACHY shows limited sensitivity to the SAA and resolves the biomass burning / lightning O₃
198 sources detected by OMI over South America, South Atlantic and Africa (18.0-20.0 DU in JJA). However,
199 especially in the NH in DJF, there appears to be regions of latitudinal banding in the L_{TCO₃} spatial patterns
200 (e.g. 0°-30°N), which are not observed (or to the same extent) as the other UV-Vis sounders. Overall, GOME-
201 2 and OMI are in good agreement spatially and seasonally with similar absolute L_{TCO₃} values. In DJF and JJA,
202 OMI appears to be 2.0-3.0 DU lower and larger than GOME-2, respectively. This is reasonable given the
203 similar temporal records they cover (2005-2017 vs. 2007-2018). SCIAMACHY has similar spatial-seasonal
204 patterns but has systematically larger (3.0-5.0 DU) DJF values in comparisons to OMI and GOME-2.

205 3.3. Satellite Instrument Temporal Stability

206 For accurate assessment of satellite L_{TCO₃} temporal variability, there needs to be insignificant drift over
207 time, whereas bias which is constant over time can be tolerated. The most appropriate data set with which
208 to assess satellite long-term drifts is that of the ozonesonde record, albeit that it has certain limitations



209 potentially including temporal changes in accuracy (Stauffer et al., 2020) as well as geographical coverage.
210 **Figure 4** shows annual time series of the satellite-ozonesonde (with AKs applied) median biases for three
211 latitude bands: 90°-30°S, 30°S-30°N and 30-90°N. The hatched pixels show where the biases are non-
212 substantial, defined as the 25_75% difference range intersecting with zero. For GOME-1, the mean bias (MB)
213 is -5.34, -3.21 and -0.90 DU for the three regions, respectively. For the 30-90°N region, several years show
214 substantial biases of -6.0 to -3.0 DU. The two other latitude bands have few substantial years but in the
215 tropical band, both 2002 and 2003 show substantial biases of approximately -5.0 DU. To assess the stability
216 of the instruments with time, a simple linear least-squares fit was performed with regional trends of -0.32, -
217 0.98* and -0.03 DU/yr. A significant trend (shown by an asterisk) at the 95% confidence level is defined as
218 $|M/\sigma_M| > 2.0$ (e.g. Pope et al., 2018), where M and σ_M are the linear trend and trend uncertainty,
219 respectively. While, the 30-90°N region had a sizable systematic bias, it was stable with time, as was the bias
220 for the 90°-30°S region. However, the 2002 and 2003 biases in the 30S°-30°N region gave rise to significant
221 drift in the GOME-1 record.

222 For GOME-2, the record MB is 1.91, -5.05 and 1.64 DU for the respective latitude bands, all of which have
223 significant bias trends at 0.62*, -0.70* and 0.22* DU/yr. Therefore, the GOME-2 LTCO₃ records from this
224 processing run are not stable and cannot be used further in the study. SCIAMACHY has regional mean biases
225 of 1.33, 4.47 and 2.81 DU. In the 30-90°N region, the bias is not significant. While there are substantial biases
226 peaking at 3.0-5.0 DU in the 90°-30°S region, neither region has a significant drift trend. The largest
227 substantial biases are in the 30S°-30°N region (>5.0 DU) for 2006 to 2008. While the positive trend of 0.21
228 DU/yr is insignificant, we do not use the SCIAMACHY data in later years when harmonising the LTCO₃ records
229 (section 3.4). OMI has MBs of -5.16, -2.91 and -0.41 DU with only a few of the year-latitude pixels having
230 substantial biases peaking at -6.0 to -3.0 DU in the 30-90°N region. The resulting bias trends are -0.12, 0.22
231 and -0.10 DU/yr, which are all insignificant. Therefore, GOME-1, OMI and SCIAMACHY were deemed suitable
232 LTCO₃ records for use in this study.

233 3.4. Lower Tropospheric Column Ozone Merged Record

234 The RAL Space products cover the full period between 1996 and 2017. Therefore, there is the opportunity to
235 merge and harmonise these records to produce a long-term record to look at the spatiotemporal variability
236 of LTCO₃. From **Figure 4**, the OMI record appears to be stable with time globally, providing a suitable data set
237 between 2005 and 2017. The GOME-2 record appears not to be sufficiently stable across its record (2008-
238 2018), so is not included in subsequent analysis. The GOME-1 record covers 1996 to 2010, but given the loss
239 of geographical coverage due to the onboard tape recorder failing in June 2003 (van Roozendaal, 2012), a
240 true global average is only available between 1996 and 2003. **Figure 4** shows that GOME-1 bias with respect
241 to the ozonesonde record is not stable in the tropics but this is predominantly driven by instrument-
242 ozonesonde differences in 2003. Therefore, 2003 is also dropped leaving the GOME-1 global record between
243 1996 and 2002.

244 While OMI (2005-2017) and GOME-1 (1996-2002) now cover a large proportion of the global record, there is
245 still a systematic difference between them. Different UV-Vis instruments can have inconsistencies in their
246 retrieved products (e.g. van der A et al., (2006), Heue et al., (2016)) and often require a systematic
247 adjustment to create a harmonised record. Here, there is overlap in the raw records between 2005 and 2010
248 for GOME-1 and OMI. The GOME-1 record does have large missing data gaps globally, but for the mid-
249 latitude and tropical latitude bands, there is sufficient sampling to inter-compare the two records. Therefore,
250 for each swath, the nearest OMI retrieval is co-located to that of GOME-1, but has to be within 250 km. The
251 local overpass times are different (i.e. GOME-1 10.30 and OMI 13.30) but within approximately 3-hours, so
252 the diurnal cycle impacts are likely to be of a secondary order and we are confident in merging the records.



253 Based on the co-located OMI and GOME-1 data, we derived long-term latitude-month offset which are
254 added to GOME-1 (1996-2002) to harmonise the records. This was done using latitudinal bins of 60°S-30°S,
255 30°S-30°N and 30°N-60°N. Given the lack of GOME-1 data outside of 60°S-60°N due to the failure of the
256 GOME-1 tape recorder in June 2003, there was insufficient data to derive offsets, the high-latitudes data is
257 excluded in the following sections. Where there was good spatial coverage from GOME-1 between 2005 and
258 2010, once the offset had been applied, gridded OMI and GOME-1 where data existed for both, on a pixel by
259 pixel basis, were averaged together.

260 For 2003 and 2004, we use the SCIAMACHY spatial fields to gap fill the record. **Figure 4** shows that
261 SCIAMACHY had some substantially large biases compared to the ozonesondes in 2006, 2007 and 2008 but
262 was reasonable for other years. Therefore, we use the global distributions from SCIAMACHY for both years
263 but scale them to expected values between 2002 and 2005. This is achieved by getting the globally weighted
264 (based on surface area) LT_{CO₃} average for GOME-1 (2002 with GOME-1 VS. OMI offset applied) and OMI
265 (2005) and the SCIAMACHY for its respective years. Based on the difference between 2002 and 2005, a
266 global scaling is applied in 2003 and 2004 for the SCIAMACHY spatial fields. Thus, we have developed a
267 harmonised LT_{CO₃} record between 1996 and 2017. Examples of the harmonised data for Europe and East
268 Asia are shown in **Figure 5**. Overall, there is non-linear variability in the two regional time-series where red
269 and blue show the GOME-1 and OMI LT_{CO₃} time series and then black shows where they have been merged.
270 For Europe (East Asia), the seasonal cycle ranges between 10.0 (13.0) and 30.0 (27.0) DU, respectively, with
271 annual average values between 18.0 (18.0) and 22.0 (21.0) DU.

272 **3.5. Lower Tropospheric Column Ozone Temporal Variability**

273 The harmonised RAL Space data set can now be used to investigate decadal scale spatiotemporal variability
274 in LT_{CO₃}. **Figure 6** shows the global long-term (1996-2017) average in LT_{CO₃} and the 5-year average
275 anomalies for 1996-2000, 2005-2009 and 2013-2017. In the long-term average (**Figure 6a**), there is clear SH
276 to NH LT_{CO₃} gradient with background values of 13.0-17.0 DU and 20-23.0 DU, respectively. There are
277 hotspots over East Asia, the Middle East/Mediterranean and northern India of 24.0-25.0 DU. The largest SH
278 LT_{CO₃} values (20.0-22.0 DU) are between 30-15°S spanning southern Africa, the Indian Ocean and Australia.
279 Minimum LT_{CO₃} values (<12.0 DU) are over the Himalayas (due to topography) and the tropical oceans.
280 Note, the SAA has been masked out in all the panels. The 1996-2000 anomaly map (**Figure 6b**) shows values
281 to be similar (i.e. -1.0 to 1.0 DU) with respect to the 1996-2017 mean between 30°N and 60°N. A similar
282 relationship occurs at approximately 30°S. However, in tropics and NH sub-tropics (15°S to 30°N), the
283 anomalies are more negative, ranging between approximately -3.0 and -1.0 DU. The green polygon-outlined
284 regions show where the 1996-2000 LT_{CO₃} average represents a significant difference (95% confidence level)
285 from the long-term average. This is based on the Wilcoxon rank test (WRT), which is the nonparametric
286 counterpart of the Student t-test that relaxes the constraint on normality of the underlying distributions
287 (Pirovano et al., 2012). As well as this tropical band, the 60-45°S band shows significant anomalies of a similar
288 magnitude. In the 2005-2009 anomaly map (**Figure 6c**), there are widespread, though insignificant,
289 anomalies of -1.5.0 to 0.0 DU. There are a scattering of significant anomalies (e.g. southern Africa at -2.0 to -
290 1.0 DU and over the Bering Sea between 1.0 and 2.0 DU) but with limited spatial coherence. In the 2013-
291 2017 anomaly map (**Figure 6d**), there remain small LT_{CO₃} anomalies in the northern mid-latitudes (-1.0 to
292 1.0 DU). A similar pattern occurs in the southern sub-tropics and mid-latitudes, though the anomalies are
293 larger peaking at 1.5 DU around 60-45°S (some are significant). However, in the tropics and sub-tropics
294 (15°S-30°N), there are significant positive anomalies of 1.0 to 2.0 DU throughout the region, peaking at 2.0-
295 2.5 DU over Africa.



296 Overall, these anomalies suggest there has been limited change in LTCO₃, between 1996 and 2000, in the NH
297 mid-latitudes (e.g. as can be seen for Europe and East Asia in **Figure 5**). Unfortunately, the SAA masks any
298 useful information on LTCO₃ over South America, but generally there has been a moderate LTCO₃ increase in
299 the SH mid-latitudes. The largest and most substantial changes have been in the tropics and sub-tropics (i.e.
300 15°S to 30°N) switching from significant negative anomalies (-2.0 to -1.0 DU) in the 1996-2000 LTCO₃ average
301 to positive anomalies (1.0-2.0 DU) in the 2013-2017 LTCO₃. **Figure 7** shows the difference between the 2013-
302 2017 and 1996-2000 averages. Over the tropics/sub-tropics (15°S-30°N), the largest significant increases of
303 3.0 to 5.0 DU occur peaking Africa, India and South-East Asian (>5.0 DU). Thus showing a large-scale increase
304 in tropical LTCO₃ between 1996 and 2017. In the NH mid-latitudes, the absolute LTCO₃ differences are
305 relatively small (-1.0 to -1.5 DU) but there are consistent, though some negative differences (generally -2.0
306 and -1.0 DU) are over North America and Russia. In the SH mid-latitudes, there has been a significant,
307 moderate increase in LTCO₃ of 2.0-3.5 DU. However, southern Africa shows more localised decreases of up
308 to 3.0 DU and non-significant differences at 30°S across the Indian Ocean.

309 **4. Discussion and Conclusions**

310 Multiple studies have used satellite records to investigate change in TCO₃ in recent decades. Gaudel et al.,
311 (2018) used a range of UV-Vis and IR TCO₃ products between 2005 and 2016. The UV-Vis sounders generally
312 show substantial significant positive trends (0.1-0.8 DU/yr) in the tropics/sub-tropics and a mixed response
313 in the mid-latitudes. The IR instruments typically showed significant decreasing trends (-0.5 to -0.2 DU/yr) in
314 background regions and isolated regions of substantial TCO₃ enhancements. Ziemke et al., (2019) used a
315 long-term merged record of TCO₃ from the Total Ozone Mapping Spectrometer (TOMS) and Ozone
316 Monitoring Instrument/Microwave Limb Sounder (OMI-MLS) between 1979 and 2016. Over this period, they
317 found significant increases of TCO₃ of 1.5 to 6.5 DU, especially over India and East Asia. Heue et al., (2016)
318 used a long-term tropical TCO₃ record (GOME, SCIAMACHY, OMI, GOME-2A and GOME-2B) finding
319 significant increases (0.5-2.0 DU/decade) over central Africa and the South Atlantic. However, the study by
320 Wespes et al., (2018) indicates that TCO₃ has been significantly decreasing between 2008 and 2017 at -0.5 to
321 -0.1 DU/yr from IASI (i.e. an IR sounder). Therefore, studies using IR products tend to show significant
322 negative trends globally, while studies using UV-Vis products show significant increasing trends in the
323 tropics/sub-tropics.

324 In this study, for the first time we analysed long-term changes in LTCO₃ using a merged satellite UV-Vis
325 sounder record. Overall, we found that LTCO₃ was lower (by 1.0-3.0) in the tropics between 1996 and 2000
326 in comparison to the long-term average (i.e. 1996-2017). Similar LTCO₃ values exist between the 2005-2009
327 and long-term averages, while the 2013-2017 average shows significantly larger tropical values (1.0-2.5 DU)
328 than the long-term average. Therefore, this tropical increase (3.0-5.0 DU) in LTCO₃ between 1996 and 2017 is
329 consistent with other reported increases in TCO₃. A similar consistency is found in the NH mid-latitudes, with
330 insignificant changes in LTCO₃ observed here and in trends in TCO₃ reported in Gaudel et al., (2018) and
331 Ziemke et al., (2019). Significant LTCO₃ increases in the SH mid-latitudes are also consistent with Gaudel et
332 al., (2018) and Ziemke et al., (2019), though they differ from IASI retrieved TCO₃ trends as reported by
333 Wespes et al (2018). Overall, the long-term changes in LTCO₃ reported here and the literature TCO₃ trends
334 from satellite UV products are comparable in regard to latitude dependence and direction. It therefore
335 seems that the positive tendencies in TCO₃ reported in the literature from UV soundings over the satellite-
336 era are associated with, and could be driven by, changes occurring in LTCO₃.

337 For future work, a detailed study is required to disentangle the reported TCO₃ and LTCO₃ trends reported by
338 UV-Vis and IR sounders, which would benefit from satellite level-2 data produced from level-1 data sets
339 which are more uniform over time along with other improvements. This can potentially be done also by



340 using a 3D atmospheric chemistry model (ACM) to investigate the changes in lower and upper tropospheric
341 ozone, and application of the satellite AKs (i.e. the vertical sensitivity of the different satellite products) to
342 the model from the different sounders to establish how satellite vertical sensitivity potentially changes the
343 simulated TO₃ tendency of the model. An ACM would also be a useful tool to help diagnose the importance
344 of LTCO₃ contributions to the TCO₃ tendencies, and which processes might be driving any spatiotemporal
345 changes (e.g. surface emissions, atmospheric chemistry/surface deposition, stratospheric-tropospheric O₃
346 exchanges etc.). Finally, together with improved, extended reprocessed versions of the data sets used in this
347 study, the launch of the Sentinel 5 – Precursor (S5P) satellite (in October 2017) can be used to extend the
348 merged data record of LTCO₃, along with new polar orbiting platforms such as Sentinel-5 and IASI-NG
349 instruments on future EUMETSAT MetOp-Second Generation satellites.

350 **Acknowledgements:**

351 This work was funded by the UK Natural Environment Research Council (NERC) by providing funding for the
352 National Centre for Earth Observation (NCEO, award reference NE/R016518/1) and funding from the
353 European Space Agency (ESA) Climate Change Initiative (CCI) post-doctoral fellowship scheme (contract
354 number 4000137140). Anna Maria Trofaier (ESA Climate Office) provided support and advice throughout the
355 fellowship.

356 **Conflicting Interests**

357 The authors declare that they have no conflicts of interest.

358 **Data Availability**

359 The RAL Space satellite data is available via the NERC Centre for Environmental Data Analysis (CEDA) Jasmin
360 platform subject to data requests. The RAL Space satellite data will be uploaded to the Zenodo open access
361 portal (<https://zenodo.org/>) if this manuscript is accepted for publication in ACP after the peer-review
362 process. The ozonesonde data for WOUDC, SHADOZ and NOAA is available from <https://woudc.org/>,
363 <https://tropo.gsfc.nasa.gov/shadoz/> and <https://gml.noaa.gov/ozwv/ozsondes/>.

364 **Author Contributions**

365 RJP, MPC and BJK conceptualised and planned the research study. RJP and MAP analysed the satellite data
366 provided by RAL Space (BJK, RS, BGL) with support from BJK, RS and BGL. MPC, SD and CR provided scientific
367 advice, while WF and RR provided technical support. RJP prepared the manuscript with contributions from
368 all co-authors.

369 **References:**

- 370 Boersma KF, et al. 2011. An improved tropospheric NO₂ column retrieval algorithm for the Ozone Monitoring
371 Instrument. *Atmospheric Measurement Techniques*, **4**, 1905–1928, doi: 10.5194/amt-4-1905-2011.
- 372 Copernicus. 2021. Product Quality Assessment Report (PQAR) Ozone products – Version 2.0b, Issued by
373 BIRA-IASB/Jean-Christopher Lambert, Ref: C3S_D312b_Lot2.2.1.2_202105_PQAR_O3_v2.0b.
- 374 ESA. 2019. Climate Change Initiative. <http://cci.esa.int/ozone> (last accessed 02/05/2023).
- 375 Eskes HJ and Boersma KF. 2003. Averaging kernels for DOAS total column satellite retrievals. *Atmospheric
376 Chemistry and Physics*, **3**, 1285–1291, doi: 10.5194/acp-3-1285-2003.
- 377 Gaudel A, et al. 2018. Tropospheric Ozone Assessment Report: Present day distribution and trends of
378 tropospheric ozone relevant to climate and global atmospheric chemistry model evaluation. *Elementa*, **6**
379 **(39)**, 1-58, doi: 10.1525/elementa.291.



- 380 Gauss M, et al. 2006. Radiative forcing since preindustrial times due to ozone change in the troposphere and
381 the lower stratosphere. *Atmospheric Chemistry and Physics*, **6**, 575-599, doi: 10.5194/acp-6-575-2006.
- 382 Heue KP, et al. 2016. Trends of tropical tropospheric ozone from 20 years of European satellite
383 measurements and perspectives for the Sentinel-5 Precursor. *Atmospheric Measurement Techniques*, **9**,
384 5037-5051, doi: 10.5194/amt-9-5037-2016.
- 385 Hubert D, et al. 2016. Ground-based assessment of the bias and long-term stability of 14 limb and
386 occultation ozone profile data records. *Atmospheric Measurement Techniques*, **9**, 2497-2534, doi:
387 10.5194/amt-9-2497-2016.
- 388 Keppens A, et al. 2018. Quality assessment of the Ozone_cci Climate Research Data Package (release 2017) –
389 Part 2: Ground-based validation of nadir ozone profile data products. *Atmospheric Measurement*
390 *Techniques*, **11**, 3769-3800, doi: 10.5194/amt-11-3769-2018.
- 391 Lamarque JF, et al. 2010. Historical (1850-2000) gridded anthropogenic and biomass burning emissions of
392 reactive gases and aerosols: methodology and application. *Atmospheric Chemistry and Physics*, **10**, 7017-
393 7039, doi: 10.5194/acp-10-7017-2010.
- 394 Miles GM, et al. 2015. Tropospheric ozone and ozone profile retrieved from GOME-2 and their validation.
395 *Atmospheric Measurement Techniques*, **8**, 385-398, doi: 10.5194/amt-8-385-2015.
- 396 Myhre G, et al. 2013. Anthropogenic and Natural Radiative Forcing, in: Climate Change 2013: The Physical
397 Science Basis. Contribution of Working Group I to the Fifth Assessment Report of the Intergovernmental
398 Panel on Climate Change Cambridge University Press, Cambridge, United Kingdom and New York, NY, USA,
399 659–740.
- 400 Pope RJ, et al. 2018. Widespread changes in UK air quality observed from space. *Atmospheric Science Letters*,
401 **19:e817**, doi: 10.1002/asl.817.
- 402 Pope RJ, et al. 2020. Substantial Increases in Eastern Amazon and Cerrado Biomass Burning-Sourced
403 Tropospheric Ozone. *Geophysical Research Letters*, **47 (3)**, e2019GL084143, doi: 10.1029/2019GL084143.
- 404 Pirovano G, et al. 2012. Investigating impacts of chemistry and transport model formulation on model
405 performance at European scale. *Atmospheric Environment*, **59**, 93-109, doi:
406 10.1016/j.atmosenv.2011.12.052.
- 407 Richards NAD, et al. 2013. The Mediterranean summertime ozone maximum: global emission sensitivities
408 and radiative impacts. *Atmospheric Chemistry and Physics*, **13**, 2231-2345, doi: 10.5194/acp-13-2331-2013.
- 409 Rodgers, C.D. 2000. Inverse methods for atmospheric sounding: Theory and practice. New Jersey, USA:
410 World Science.
- 411 Shah S, et al. 2018. Evaluation of SCIAMACHY Level-1 data versions using nadir ozone profile retrievals in the
412 period 2003-2011, *Atmospheric Measurement Techniques*, **11**, 2345-2360, doi: 10.5194/amt-11-2345-2018.
- 413 Sitch S, et al. 2007. Indirect radiative forcing of climate change through ozone effects on the land-carbon
414 sink. *Nature*, **448**, 791-794, doi: 10.1038/nature06059.
- 415 Stauffer RM, et al. 2020. A post-2013 Dropoff in Total Ozone at a Third of Global Ozone-sonde Stations:
416 Electrochemical Concentration Cell Instrument Artefacts?, *Geophysical Research Letters*, **47 (11)**,
417 e2019GL086791, doi: 10.1029/2019GL086791.



- 418 Stevenson DS, et al. 2013. Tropospheric ozone changes, radiative forcing and attribution to emissions in the
419 Atmospheric Chemistry and Climate Model Intercomparison Project (ACCMIP), *Atmospheric Chemistry and*
420 *Physics*, **13**, 3063- 3085, doi: 10.5194/acp-13-3063-2013.
- 421 van der A, et al. 2006. Detection of the trend and seasonal variation in tropospheric NO₂ over China. *Journal*
422 *of Geophysical Research*, **11**, D12317, doi: 10.1029/2005JD006594.
- 423 Van Roozendael M, et al. 2012. Sixteen years of GOME/ERS-2 total ozone data: The new direct-fitting GOME
424 Data Processor (GDP) version 5—Algorithm description. *Journal of Geophysical Research: Atmospheres*, **117**,
425 D03305, doi: 10.1029/2011JD016471.
- 426 Verstraeten WW, et al. 2015. Rapid increase in tropospheric ozone production and export from China.
427 *Nature Geoscience*, **8**, 690-695, doi: 10.1038/NGEO2493.
- 428 Wespes C, et al. 2018. Decrease in tropospheric levels in the Northern Hemisphere observed by IASI.
429 *Atmospheric Chemistry and Physics*, **18**, 6867-6885, doi: 10.5194/acp-18-6867-2018.
- 430 Young PJ, et al. 2013. Pre-industrial to end 21st century projections of tropospheric ozone from the
431 Atmospheric Chemistry and Climate Model Intercomparison Project (ACCMIP). *Atmospheric Chemistry and*
432 *Physics*, **13**, 2063-2090, doi: 10.5194/acp-13-2063-2013.
- 433 Ziemke JR, et al. 2006. Tropospheric ozone determined from Aura OMI and MLS: Evaluation of
434 measurements and comparison with the Global Modelling Initiative's Chemical Transport Model, *Journal of*
435 *Geophysical Research*, **111** (D19303), doi: 10.1029/2006JD007089.
- 436 Ziemke JR, et al. 2011. A global climatology of tropospheric and stratospheric ozone derived from Aura
437 OMI/MLS measurements, *Atmospheric Chemistry and Physics*, **11**, 9237-9251, doi: /10.5194/acp-11-9237-
438 2011.
- 439 Ziemke JR, et al. 2019. Trends in global tropospheric ozone inferred from a composite record of
440 TOMS/OMI/MLS/OMPS satellite measurements and the MERRA-2 GMI simulation. *Atmospheric Chemistry*
441 *and Physics*, **19**, 3257-3269, doi: 10.5194/acp-19-3257-2019.
- 442
- 443
- 444
- 445
- 446
- 447
- 448
- 449
- 450
- 451
- 452
- 453
- 454



455 **Figures & Tables:**

Data Provider	Satellite Profile Products & Version	Product Link	Data Range	Data Size
RAL Space	OMI-fv214	http://www.ceda.ac.uk/	2004-2018	1442 GB
RAL Space	GOME-2A-fv300	http://www.ceda.ac.uk/	2007-2019	1007 GB
RAL Space	GOME-1-fv301	http://www.ceda.ac.uk/	1995-2011	703 GB
RAL Space	SCIAMACHY-fv300	http://www.ceda.ac.uk/	2002-2012	718 GB

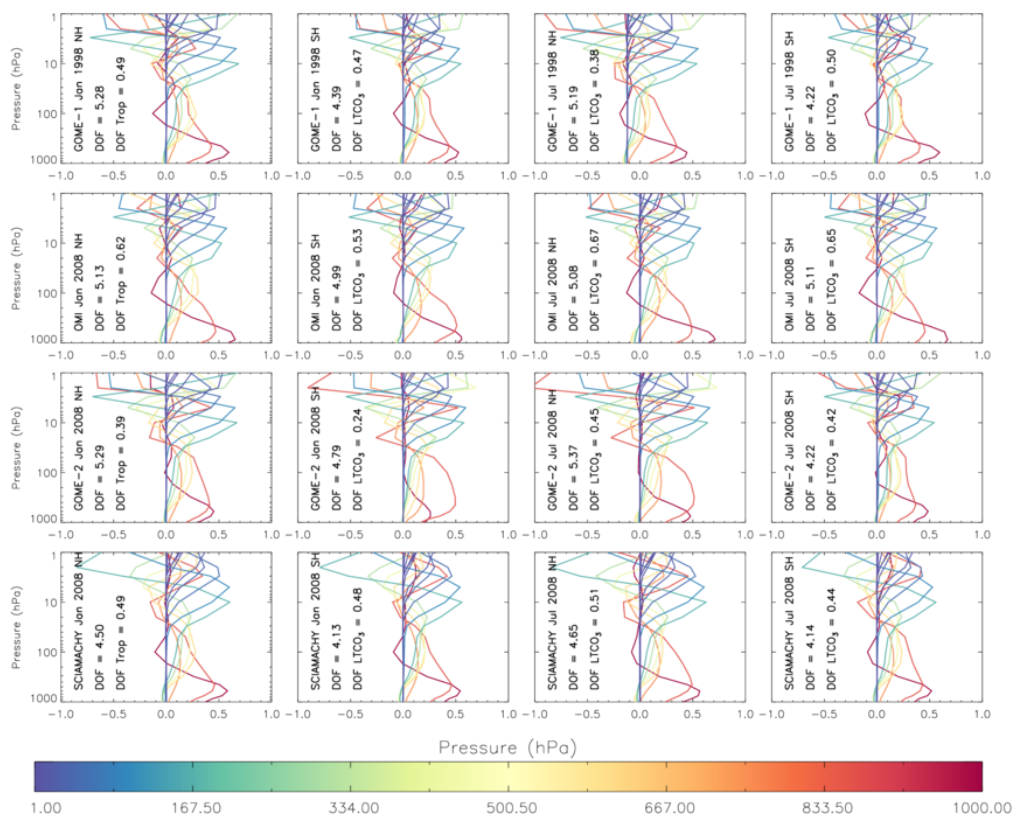
456 **Table 1:** List of RAL Space level-2 satellite ozone profile data sets.

457

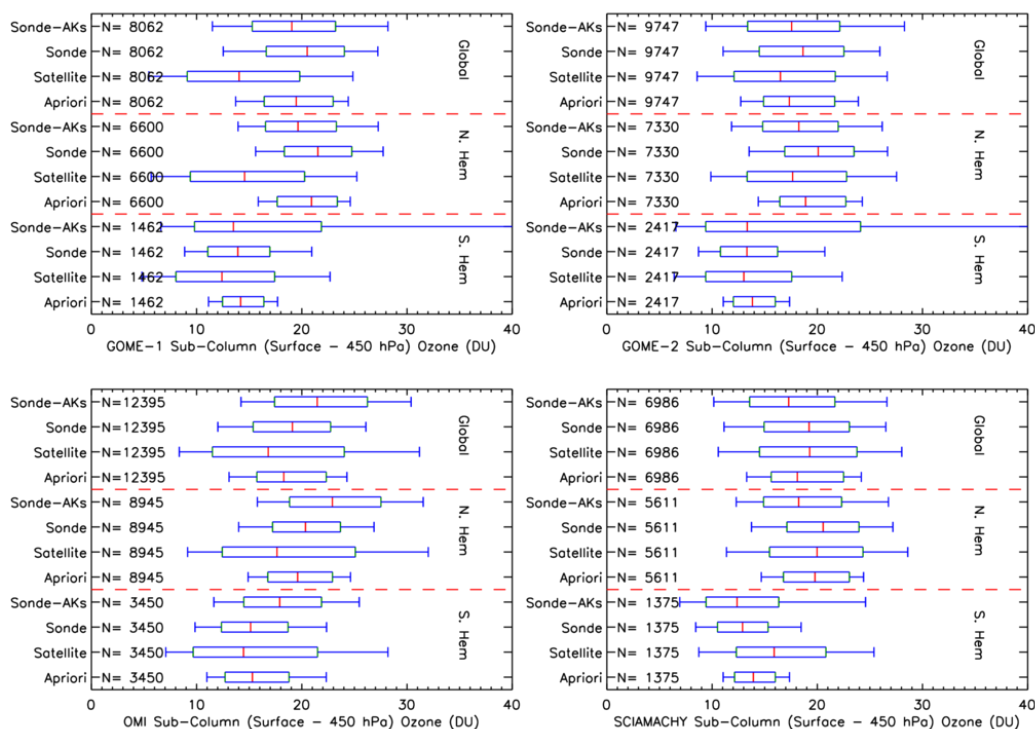
DOFS	GOME-1	OMI	GOME-2	SCIAMACHY
January 2008 NH	5.28 (0.49)	5.13 (0.62)	5.29 (0.39)	4.50 (0.49)
January 2008 SH	4.39 (0.47)	4.99 (0.53)	4.79 (0.24)	4.13 (0.48)
July 2008 NH	5.19 (0.38)	5.08 (0.67)	5.37 (0.45)	4.65 (0.51)
July 2008 SH	4.22 (0.50)	5.11 (0.65)	4.22 (0.42)	4.14 (0.44)

458 **Table 2:** Degrees of freedom of signal (DOFS) for the full ozone profile in red and the lower tropospheric
 459 column ozone (LTCO₃) layer in blue from GOME-1, OMI, GOME-2 and SCIAMACHY. These values are from the
 460 average averaging kernels (AKs, see **Figure 1**) for the Northern Hemisphere (NH) and Southern Hemisphere
 461 (SH) in January and July 2008 (1998 for GOME-1).

462
 463
 464
 465
 466

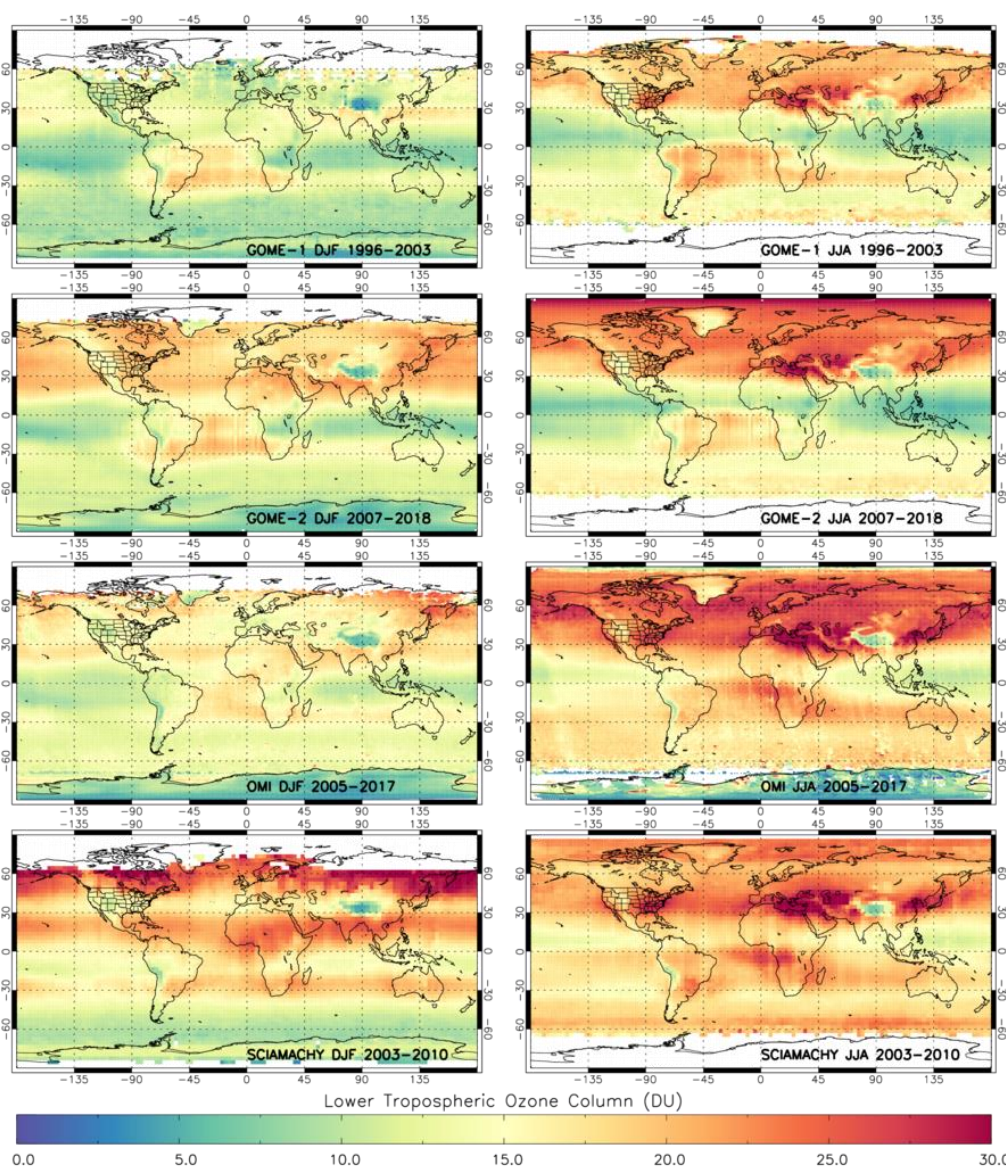


467
 468 **Figure 1:** Average averaging kernels (AKs) for the instruments listed in **Table 1** for the northern and southern
 469 hemispheres in January and July of 2008 (1998 for GOME-1). The average degrees of freedom of signal (DOF)
 470 is shown as is DOF LTCO₃ which represents the DOFs in the lower tropospheric column ozone (LTCO₃).



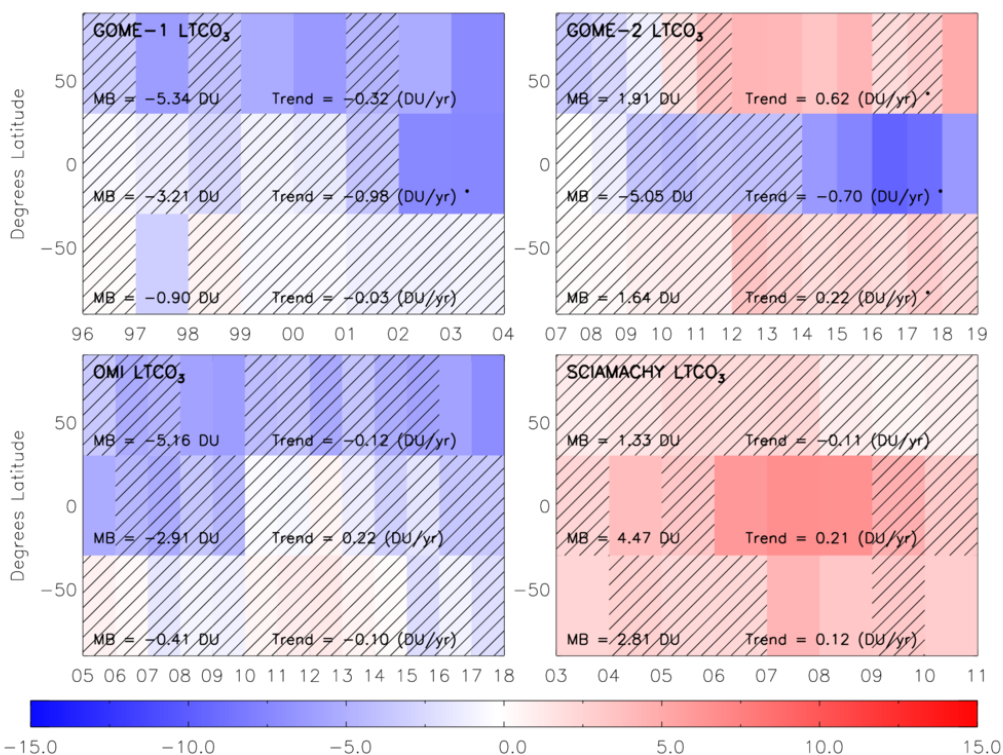
471
 472 **Figure 2:** Box and whisker distributions of $LTCO_3$ from satellite, apriori, ozonesonde (Sonde) and ozonesonde
 473 with AKs applied (Sonde-AKs) for co-located samples (i.e. satellite and ozonesonde profiles co-located within
 474 6-hours and 500 km). This is done for GOME-1 (top-left), GOME-2 (top-right), OMI (bottom-left) and
 475 SCIAMACHY (bottom-right) on a global, southern hemispheric and northern hemispheric basis over their
 476 respective records. Red dashed lines separate the box and whisker distributions for each region. The red,
 477 green and blue vertical lines represent the 50th, 25th & 75th and 10th & 90th percentiles. N represents the sample
 478 size.

479
 480
 481
 482
 483
 484



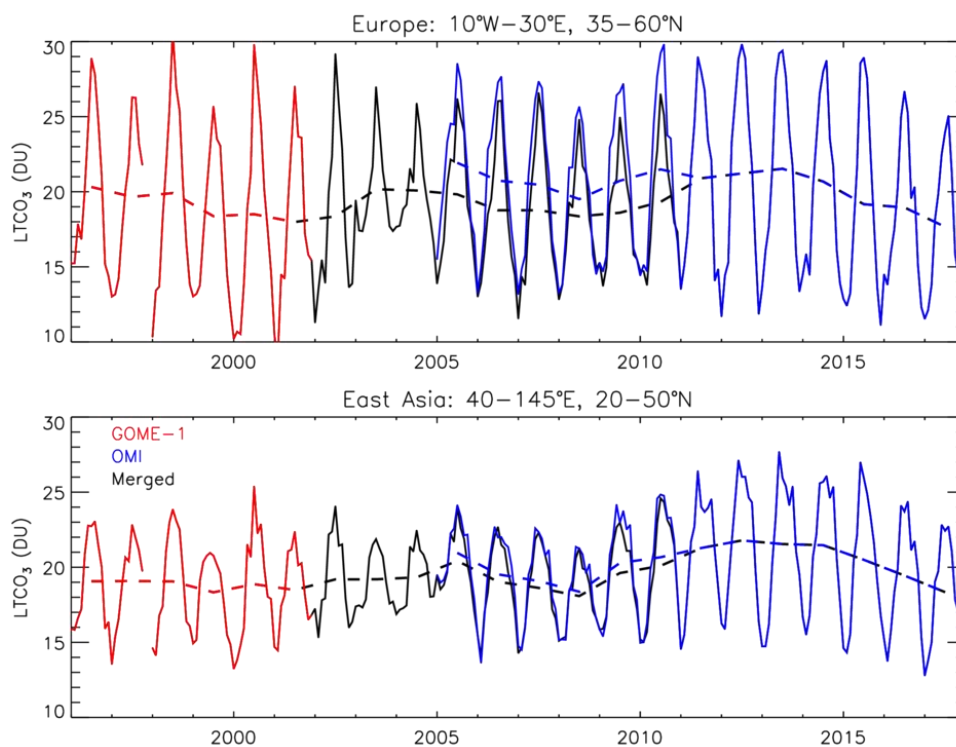
485
486
487
488
489

Figure 3: Seasonal distributions of $LTCO_3$ in December-January-February (DJF) and June-July-August (JJA) for OMI, GOME-1, GOME-2 and SCIAMACHY averaged over the full record for each instrument.



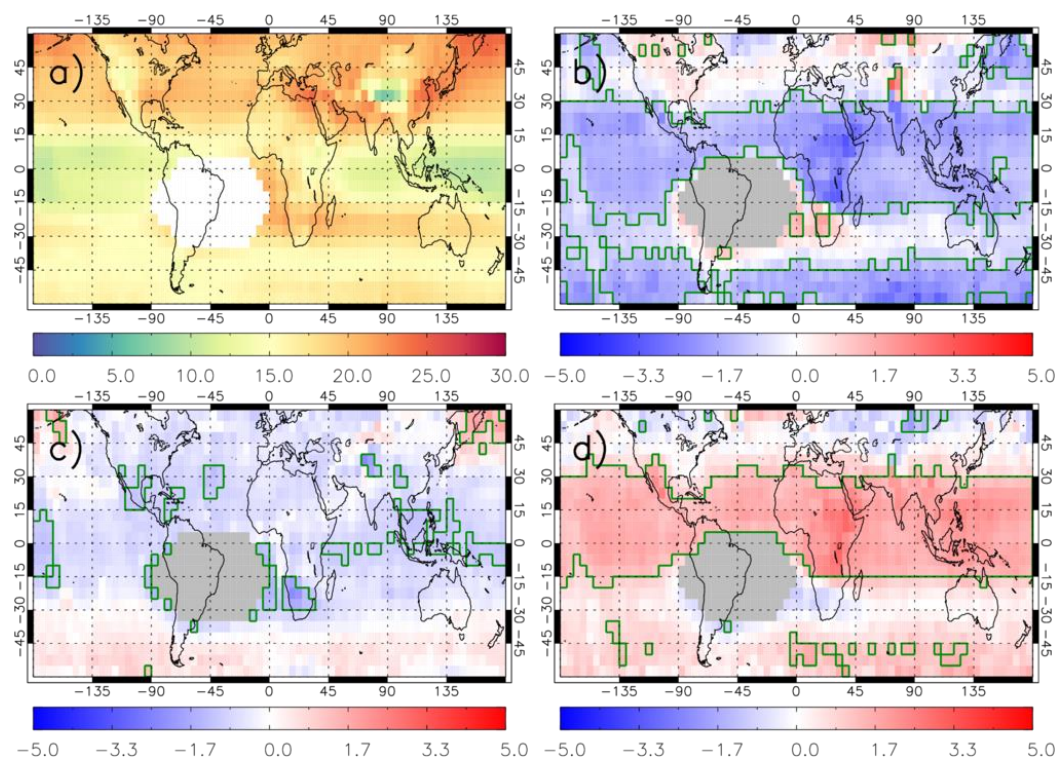
490
 491 **Figure 4:** Latitudinal-annually varying satellite-sonde, with AKs applied, LTO₃ (DU) median (50th percentile)
 492 biases. Hatched regions show where the spread in the 25th and 75th percentiles intersects with 0.0. The mean
 493 bias (MB) and trend are for the full time series of each hemisphere. The * for the trend term indicates it is
 494 significant at the 95% confidence level.

495
 496
 497
 498
 499
 500
 501
 502
 503
 504
 505
 506
 507



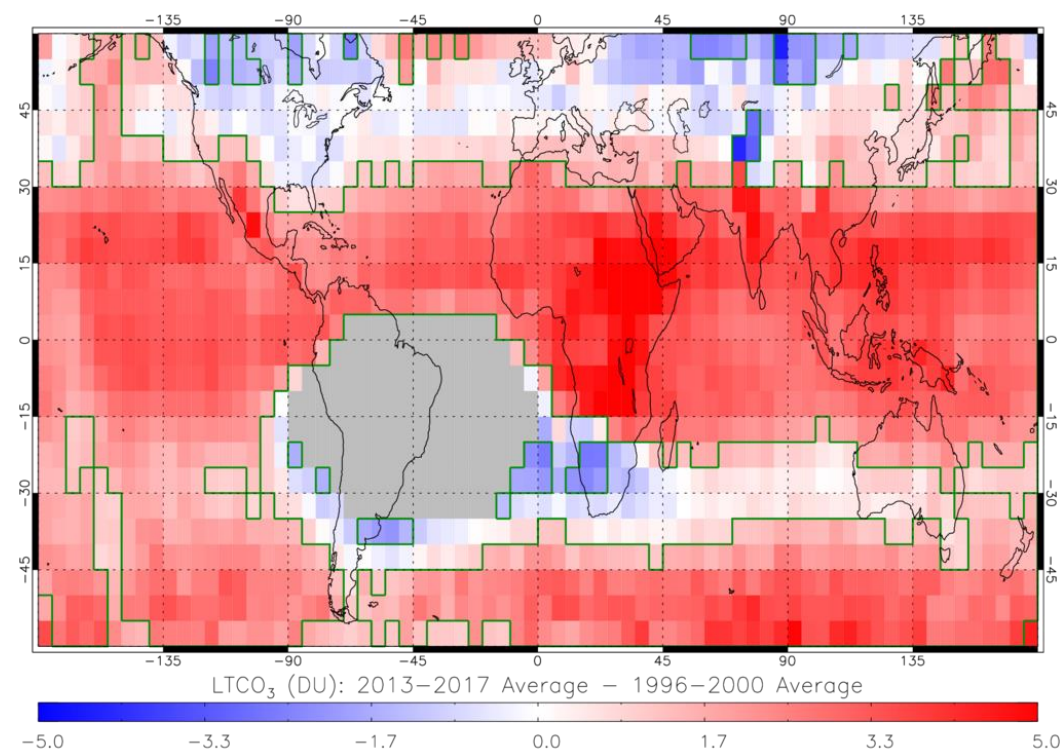
508

509 **Figure 5:** Examples of the merged LT_{CO₃} (DU) data set for Europe and East Asia. The GOME-1, OMI and
510 merged time series are shown in red, blue and black, respectively. Dashed lines represent the annual
511 averages and the monthly mean time-series are solid lines.



512

513 **Figure 6:** LTCO₃ (DU) merged data set from GOME-1 (1996-2002), SCIAMACHY (2003-2004) and OMI (2005-
514 2017). a) 1996-2017 long-term average, b) 1996-2000 average anomaly, c) 2005-2009 average anomaly and
515 d) 2013-2017 average anomaly. Anomalies are relative to the long-term average (panel a). Green polygon-
516 outlined regions show significant anomalies (95% confidence level and where the absolute anomaly > 1.0 DU)
517 from the long-term average using the Wilcoxon Rank Test. White/grey pixels are where the South Atlantic
518 Anomaly influence on retrieved LTCO₃ has been masked out.



519

520 **Figure 7:** LTCO₃ (DU) merged data set from GOME-1 (1996-2002), SCIAMACHY (2003-2004) and OMI (2005-
521 2017) where the difference between the 2013-2017 average and 1996-2000 average is shown. Green
522 polygon-outlined regions show significant differences (95% confidence level and where the absolute
523 difference > 1.0 DU) using the Wilcoxon Rank Test. Grey pixels are where the South Atlantic Anomaly
524 influence on retrieved LTCO₃ has been masked out.

525